environmental microbiology

Environmental Microbiology (2017) **19**(2), 710–721 doi:10.1111/1462-2920.13615

Metabolic response of *Agrobacterium tumefaciens* 5A to arsenite

Monika Tokmina-Lukaszewska,[1†] Zunji Shi,[1,2†] Brian Tripet,[1] Timothy R. McDermott,[3] Valérie Copié,[1] Brian Bothner[1*] and Gejiao Wang[2]**

[1]*Department of Chemistry and Biochemistry, Montana State University, Bozeman, MT 59717, USA.*

[2]*State Key Laboratory of Agricultural Microbiology, College of Life Science and Technology, Huazhong Agricultural University, Wuhan 430070, P. R. China.*

[3]*Department of Land Resources and Environmental Sciences, Montana State University, Bozeman, MT 59717, USA.*

Summary

Wide-spread abundance in soil and water, coupled with high toxicity have put arsenic at the top of the list of environmental contaminants. Early studies demonstrated that both concentration and the valence state of inorganic arsenic (arsenite, As(III) vs. arsenate As(V)) can be modulated by microbes. Using genetics, transcriptomic and proteomic techniques, microbe-arsenic detoxification, respiratory As(V) reduction and As(III) oxidation have since been examined. The effect of arsenic exposure on whole-cell intracellular microbial metabolism, however, has not been extensively studied. We combined LC-MS and ^{1}H NMR to quantify metabolic changes in *Agrobacterium tumefaciens* (strain 5A) upon exposure to sub-lethal concentrations of As(III). Metabolomics analysis reveals global differences in metabolite concentrations between control and As(III) exposure groups, with significant perturbations to intermediates shuttling into and cycling within the TCA cycle. These data are most consistent with the disruption of two key TCA cycle enzymes, pyruvate dehydrogenase and α-ketoglutarate dehydrogenase. Glycolysis also appeared altered following As(III) stress, with carbon accumulating as complex saccharides. These observations suggest that an important consequence of As(III) contamination in nature will be to alter microbial carbon metabolism at the microbial community level and thus has the potential to foundationally impact all biogeochemical cycles in the environment.

Received 26 August, 2016; revised 24 October, 2016; accepted 16 November, 2016. For correspondence. *E-mail bbothner@chemistry.montana.edu; Tel. (+1) 406 994 5270; Fax (+1) 406 994 5407. **E-mail gejiao@mail.hzau.edu.cn; Tel. (+86) 27 87281261; Fax (+86) 27 87280670. †These two authors contributed equally to this work.

Introduction

Interest and concomitant progress in understanding microbe-arsenic interactions have grown substantially over the past approximate decade. Early physiology and genetic studies focused on an arsenic detoxification model featuring the *ars* genes (Mukhopadhyay *et al.*, 2002; Rosen, 2002). In the most general terms, this involves arsenate [As(V)] accessing the cell cytoplasm via a phosphate transporter, being reduced by an As(V) reductase (ArsC) to the more toxic arsenite [As(III)], which is then actively transported out of the cell by antiporters (ArsB or Acr3). Important discoveries have followed, illustrating that a different As(V) reductase (ArrBA) could couple As(V) reduction to anaerobic respiration and energy generation (Saltikov and Newman, 2003). The *arrAB* genes and their regulation, as well as electron transport have since been described in some detail (Murphy and Saltikov, 2007; 2009; Reyes *et al.*, 2010). Similar progress has been made regarding As(III) oxidase, which is encoded by *aioBA* (Muller *et al.*, 2003), and functions as a detoxification mechanism (Osborne and Ehrlich, 1976; Phillips and Taylor, 1976) or to generate energy (Santini *et al.*, 2000; Wang *et al.*, 2015). This oxidase is regulated by a three component signal transduction system AioXSR and RpoN (Kashyap *et al.*, 2006; Koechler *et al.*, 2010; Kang, Bothner, *et al.*, 2012; Liu *et al.*, 2012). In addition, elements of the phosphate stress response (PhoRB) are varyingly involved depending on the organism (Kang, Heinemann, *et al.*, 2012; Chen *et al.*, 2015).

Central themes of microbial cellular arsenic responses have begun to emerge from proteomics and transcriptomics studies (Parvatiyar *et al.*, 2005; Carapito *et al.*, 2006; Weiss *et al.*, 2009; Cleiss-Arnold *et al.*, 2010; Andres *et al.*, 2013). Induction of *ars*, *arr* and *aio* genes occurs in response to As(III) (Kashyap *et al.*, 2006; Cleiss-Arnold *et al.*, 2010; Andres *et al.*, 2013). However, elements of an

oxidative stress response are also quite evident in *Pseudomonas aeruginosa* (Parvatiyar *et al*., 2005), as well as other bacteria (Abdrashitova *et al*., 1990; Ji and Silver, 1992) and mammalian systems (e.g., (Hall *et al*., 1997; Ochi, 1997; Jomova *et al*., 2011). While the exact mechanism of how reactive oxygen species (ROS) are generated in response to As(III) exposure remains speculative (Shi *et al*., 2004); it is known that As(III) aggressively attacks sulfhydryl groups. This is suspected to rapidly inactivate reduced glutathione, which is a primary antioxidant in cells, rendering the cell susceptible to damage resulting from normal levels of ROS generated by aerobic metabolism. Progress notwithstanding, the specific influence of arsenic on the microbial cellular metabolome *per se* has received only limited attention thus far (Jain *et al*., 2012) and in complex experimental settings wherein the effects of arsenic *per se* may be difficult to parse out (Lu *et al*., 2014). Herein we summarize the results of experiments using integrated MS and ^{1}H-NMR metabolomics approaches to examine how and to what extent cellular metabolite pools are influenced by bacterial cellular exposure to As(III).

Results

LC-MS analysis of metabolic changes in response to as(III)

Our previous efforts illuminated how *aioSRBA* expression is suppressed by high phosphate (Pi) (Kang, Heinemann, *et al*. 2012). Therefore, in this study 50 μM Pi was present in the growth media to achieve an active growth state, followed by transition to a Pi stress condition at approximately 4 h, then by an additional 2 h to achieve full induction of the *aioBA* genes (Kang, Heinemann, *et al*., 2012) and *ars* genes (Kang *et al*., 2016). It is thus reasonable to assume that under these growth conditions, full induction of As(III)-sensitive genes is well underway and that As(III)-sensitive enzymes are likewise influenced. Cells were harvested 6 h after exposure to 100 μM As(III) and metabolites were extracted. The experimental reproducibility for the five biological replicates was good, and encompassed culturing, cell lysis, metabolite extraction and analysis. LC-MS conditions specific for polar and non-polar metabolites were used to ensure significant coverage of the *Agrobacterium tumefaciens* metabolome, illustrating differences for both polar and non-polar fractions after exposure to As(III) (Fig. 1). Approximately 2300 polar features were detected in each of the replicates with and without As(III)-treatment (Fig. 2). Reverse-phase LC detected twice as many molecules in each sample. An overall comparison of the extent to which As(III) alters the cellular metabolite profiles was made using volcano plots. This revealed that roughly three times more non-polar features increased versus decreased in abundance, while changes in the polar metabolite pool were more balanced (Fig. 3). From the pool of metabolites that were significantly changed by exposure to As(III) (p-value ≤ 0.05, fold-change > 1.5), 12 could be identified. These were primarily carbohydrates and amino acids, with increases ranging from 1.5- to 8-fold and decreases up to 5-fold (Table 1).

Metabolite profiling using ^{1}H NMR spectroscopy

Metabolite extracts were profiled by recording ^{1}H NMR spectra on a 600 MHz Bruker AVANCE III NMR spectrometer. A representative one-dimensional spectrum is shown in Fig. 4. In all NMR spectra, signals originating from mono and poly saccharides (3.4–4.0 ppm) were highest in intensity. Less intense signals were observed for aliphatic (0.5–3.4 ppm) and aromatic (6–8 ppm) protons. Based on comparison of peak intensity, multiplicity and chemical shifts with standard compounds observed in the Chenomx™ 600 MHz library, 36 metabolites were identified unambiguously and quantified. The majority of detected metabolites corresponded to amino acids, sugars and a few organic acids (Table 2). A comparison of the metabolites concentrations between As(III) stressed and control samples established that 26 of the identified metabolites were higher in concentration in the As(III) stressed group. Unsupervised PCA analysis was performed as a means of visualizing the differences between control and As(III) groups. The resulting score plot showed clear separation between the two groups, with the control group much less tightly clustered than the arsenic stressed group (Fig. 5). This dispersion appears to arise from larger variations in metabolite concentrations between individual control samples. This metabolic "scatter" of the control group compared with the more tightly clustered stressed group has been seen previously, suggesting a similar response and narrowing of metabolic space when bacterial cells experience environmental stress (Heinemann, Mazurie, *et al*., 2014; Tokmina-Lukaszewska *et al*., 2014).

To further analyze the metabolic differences and identify the metabolites most responsible for the separation between control and As(III) stressed groups, a supervised partial least squares discriminant analysis (PLS-DA) was performed. A model with goodness of fit and cross-validation predictive ability was determined with good separation between control and As(III) groups. The variable influence on projection (VIP) value for each metabolite was calculated, and metabolites identified with a VIP score-≥ 1.1 are presented in Table 2. These included the amino acids alanine, glutamine, glutamate, leucine, isoleucine, phenylalanine, valine and β-alanine. Other metabolites included lactate, nicotinate, oxypurinol, putrescine, cytosine and ribose. ^{1}H NMR-based metabolomics analysis shared metabolites in common with LC-MS; lactate, alanine, putrescine, ribose and in particular glutamate, were

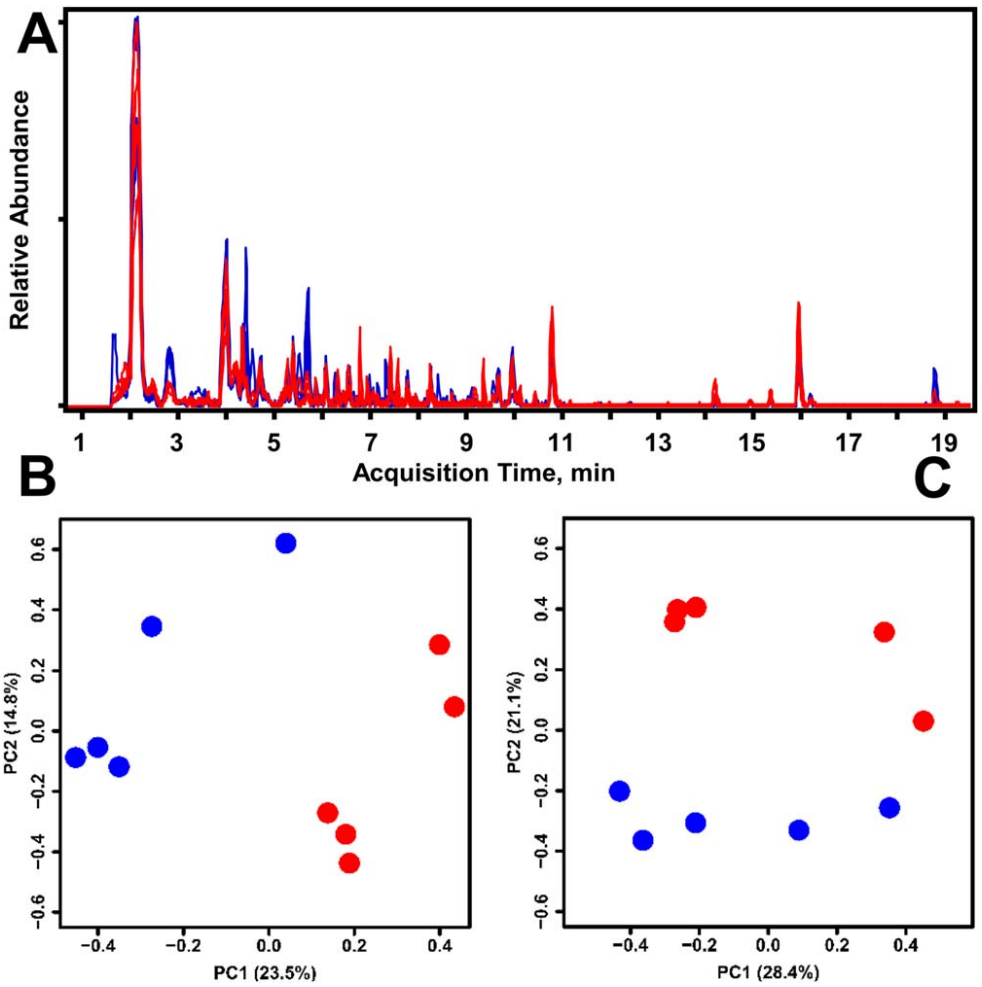

Fig. 1. LC-MS analysis of intracellular metabolites.
A. Total ion chromatogram of the C18 column (reverse-phase) illustrating varying peak intensities of features for controls cultures (blue trace) as compared with As(III) treated cells (red trace).
B. Principal component analysis of polar metabolites and (C) non-polar metabolites from control (blue dots) and As(III) exposed cultures (red dots).

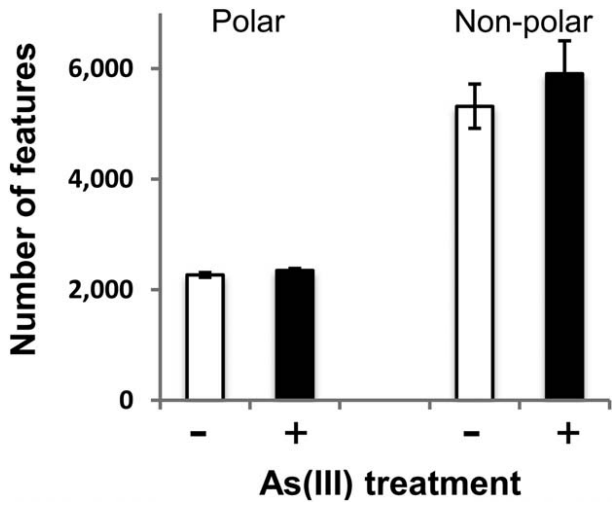

Fig. 2. Average number and variation in spectral features detected by LC-MS. Data represent five biological replicates for control and As(III)-treated cultures. Two columns were used for LC-MS analysis, HILIC to capture polar compounds and reverse-phase to capture non-polar compounds.

found to be major metabolites observed by both approaches.

Metabolites were mapped onto KEGG metabolite pathways to generate potential models of cellular pathways impacted by As(III) treatment. The metabolite data reported in Tables 1 and 2 were used to assess carbon flow beginning with mannitol as the sole carbon source in the synthetic, minimal medium used for cell culture. In this pathway analysis, the most parsimonious route of carbon flow was assumed, with mannitol catabolism entering glycolysis at the level of fructose-6-P, proceeding on to the formation of pyruvate and then terminal oxidation via the decarboxylation reactions of the tricarboxylic acid cycle (TCA) (Fig. 6). As metabolites were identified and added to the model, a pattern emerged inferring that carbon flow through the specific pathways was increased when cells were exposed to As(III). Specifically, accumulation of various metabolites (amino acids in particular) suggested the formation of "metabolic bottlenecks," involving reactions catalyzed by the enzymes pyruvate dehydrogenase and α-ketoglutarate dehydrogenase. In addition to identifying

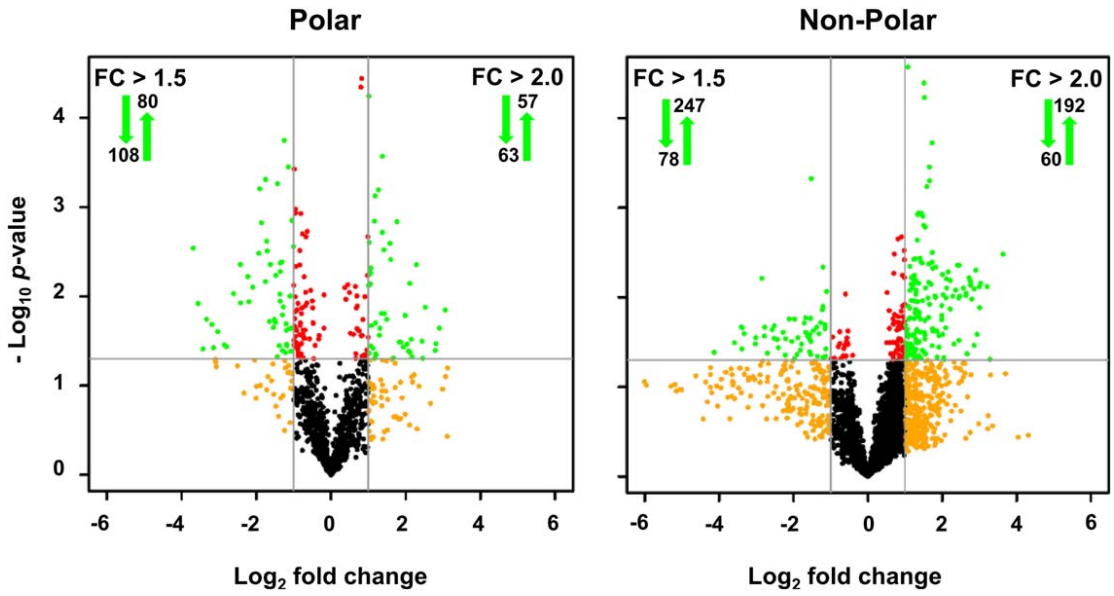

Fig. 3. MS-based analysis of global perturbation of *A. tumefaciens* cellular metabolism in response to As(III) exposure. MS features detected using hydrophilic interaction chromatography are referred to as polar metabolites, whereas features detected using C18 reverse phase chromatography are referred to as non-polar. Gray vertical lines denote the −2 and +2 fold change designated cut-off. Horizontal gray lines denote a statistical significance *p*-value ≤0.05. Green arrows refer to subset of features exhibiting 1.5- or 2.0-fold change (FC) with a *p*-value ≤0.05.

metabolites exhibiting significant changes, the LC-MS data was examined to determine if the intermediates in the suggested branches could be identified to obtain additional evidence of carbon flow through these specific pathways (defined as solid vector arrows in Fig. 6). This was the case for most, e.g., two of the four intermediates involved in the synthesis of valine from pyruvate were found, as were three of the nine intermediates involved in the synthesis of lysine from aspartate. In some cases, intermediates initiating key pathways could not be identified; however, pathways were nevertheless suggested based on accumulated evidence of key intermediates. For example, several maltose derivatives that were identified in the LC-MS spectra, suggesting that carbon originating from carbohydrate catabolism may be diverted from glycolysis for other cellular purposes. Similarly, the shikimate pathway used by microbes for the *de novo* synthesis of aromatic amino acids was inferred from the identification of significant levels of phenylalanine and tryptophan, as well as high levels of chorismate, a key downstream metabolite of this pathway. However, we could not unambiguously identify any of the nine intermediates involved in the pyruvate to leucine biosynthesis pathway, suggesting uncertainty as to whether this specific pathway is enhanced in As(III) stressed cells.

Discussion

The studies of microbe-arsenic interactions have progressed to where there is now a foundational understanding of how microbes detect and respond to arsenic. These studies have primarily concerned various major arsenic redox transformations or resistance mechanisms (Stolz and Oremland, 1999; Rosen, 2002; Oremland and Stolz, 2003; Silver and Phung, 2005) as well as non-targeted assessments of arsenic effects at more global levels using proteomics (Parvatiyar *et al.*, 2005; Carapito *et al.*, 2006; Muller *et al.*, 2007; Weiss *et al.*, 2009; Pandey *et al.*, 2012; Andres *et al.*, 2013; Belfiore *et al.*, 2013; Sacheti *et al.*, 2014; Thomas *et al.*, 2014; Ge *et al.*, 2016) and transcriptomics (Cleiss-Arnold *et al.*, 2010; Andres *et al.*, 2013; Sanchez-Riego *et al.*, 2014; Halter *et al.*, 2015). A central theme that has emerged from each study is that As(III) exposure induces bacterial functions directly related to arsenic transformations or resistance (e.g., *arsC*, *arsB* and *aioBA*.), oxidative stress response (Parvatiyar *et al.*, 2005) presumably due to loss of reduced glutathione (e.g., up-regulation of *gor*, *sod* and *kat*), as well as DNA repair activities (Bryan *et al.*, 2009; Weiss *et al.*, 2009; Cleiss-Arnold *et al.*, 2010; Li *et al.*, 2010).

Though complete concordance between transcriptional and translational change is not expected, this information is generally informative for the prediction of metabolic changes, in particular up-regulated functions. However, with the exception of proteins that recognize As(III) as their regulatory ligand, interactions between As(III) and protein thiols has a high probability of protein inactivation. These interactions are post-translational, cannot be observed at

Table 1. Metabolites identified using LC-MS. Metabolites with tentative assignment are shown in italic. Metabolites with tentative assignment were missing confirmation based on MS/MS fragmentation due to insufficient number of generated fragments or indistinguishable patterns (isomers).

Metabolite	Fold change	*p*-Value	Regulation
Betaine	4.6	0.03	Down
Cytosine	2.4	0.04	Up
D-pyroglutamate	1.8	0.00	Up
D-sorbitol	1.5	0.03	Down
Glutamate	1.8	0.00	Up
Glycerophosphocholine	1.6	0.09	Down
Hypoxanthine	8.0	0.15	Up
Isonicotinate	2.4	0.02	Up
Lysine	1.2	>0.2	Up
Maltohexaose	1.1	>0.2	Up
Maltopentaose	1.5	0.04	Up
Maltotetraose	1.9	0.01	Up
Maltotriose	2.1	0.02	Up
Phenylalanine	1.3	>0.2	Up
Proline	1.4	0.20	Down
Tryptophan	1.4	0.16	Up
Xanthine	3.5	0.02	Down
Arginine		>0.2	
Aspartate		>0.2	
Chorismate		>0.2	
Mannose		>0.2	
Sucrose		>0.2	
Valine		>0.2	

(S)−2-Acetolactate/3-hydroxy-3-methyl-2-oxobutanoate.
(R)−2,3-Dihydroxy-3methylbutanoate.
2-Oxoisovalerate.
(2S)−2-Isopropyl-3-oxosuccinate.
Pyruvate.
Nicotinate D-ribonucleoside.
N-Formyl-kynurenine.
Anthranilate.
3-hydroxy-L-kynurenine.
L−4-Aspartate semialdehyde.
LL−2,6-Diaminopimelate/meso-2,6-diaminoheptanedioate.

the transcriptional level and may not necessarily be detectable in a proteomics analysis. As such, increased gene transcription or protein abundance in reaction to As(III) exposure may not ultimately result in increased function, and thus could result in an incomplete understanding of overall global cellular responses. Complementing transcriptomics and proteomics data with metabolomics analyses provides a powerful mean to enhance our knowledge of how As(III) impacts cellular functions.

Protein thiols are subject to As(III) inactivation and if such a residue is critical to enzyme function, this will lead to interruption of a pathway whose reactions are catalyzed by such enzymes. The complete or partial inactivation of an enzyme will result in accumulation of upstream metabolites and depletion of downstream intermediates or end products. Accumulation of metabolites as a result of enzyme inactivation could divert carbon flow to other pathways, even in the absence of changes in the enzyme abundance or activity. As expected, a range of enzyme classes can be inhibited by As(III) (González-Segura *et al.*, 2009; Jain *et al.*, 2012). Specific examples relevant to the current study include documented inhibition of pyruvate dehydrogenase (PDH), α-ketoglutarate dehydrogenase (KGDH) and branched-chain α-ketoacid dehydrogenase (BCKDH) enzymes. These enzymes all contain a dihydrolipoamide dehydrogenase subunit that is sensitive to As(III) inactivation across organisms (Bergquist *et al.*, 2009; Afzal *et al.*, 2012; Chen *et al.*, 2014). Inhibition of these specific enzymes is consistent with the measured increase in abundance of several metabolites observed in As(III) exposed *A. tumefaciens* 5A (Fig. 6). Specifically, As(III) inhibition of PDH would lead to the accumulation of pyruvate, which is the precursor to the formation of lactate, leucine, isoleucine, alanine and valine. Some of these compounds are precursors for other metabolites observed to increase in abundance, such as nicotinate and isonicotinate, although these latter metabolites could also be synthesized from tryptophan. Preferential accumulation of the branched-chain amino acids leucine, isoleucine and valine could be further promoted by As(III) inhibition of BCKDH which catalyzes the catabolism of these amino acids. As(III) inhibition of KGDH would likewise lead to the preferential diversion of metabolite intermediates from TCA carbon flow and instead utilize α-ketoglutarate to form glutamate, which can be converted to glutamine, ornithine, arginine and putrescine, as well as lysine although less directly (Fig. 6). To our knowledge, the only route of D-5-oxoproline synthesis (increased abundance in As(III)) involves glutamate in an ATP-depleting futile cycle that includes γ-glutamyl phosphate (Emmett, 2014). We also note that ornithine decarboxylase activity is enhanced/stabilized by As(III) in erythroleukemia cells (Flamigni *et al.*, 1989), rat hepatic cells (Brown *et al.*, 1997) and in *Leishmania* (Haimeur *et al.*, 1999). To the extent that this also occurs in bacteria such as *A. tumefaciens* 5A, this would promote putrescine synthesis, as observed here (Fig. 6). Increased levels of pyruvate and phosphoenolpyruvate (PEP in Fig. 6) could contribute toward increased levels of oxaloacetate (PEP carboxylase or pyruvate carboxylase, are both encoded in strain 5A's genome), which can be used as precursors for the synthesis of lysine, alanine and cytosine. All of the above scenarios are consistent with a targeted study concerning As(III)-treated *Rhodococcus* that found significantly reduced enzyme levels of PDH, KGDH and malate dehydrogenase (Jain *et al.*, 2012), which corresponded to increased levels of pyruvate, α-ketoglutarate and oxaloacetate. The consistency of this study with our observations belies what might be predicted from proteomics studies that suggest increased levels of TCA cycle activity (Baker-Austin *et al.*, 2007; Bryan *et al.*, 2009; Weiss *et al.*, 2009), emphasizing the importance of

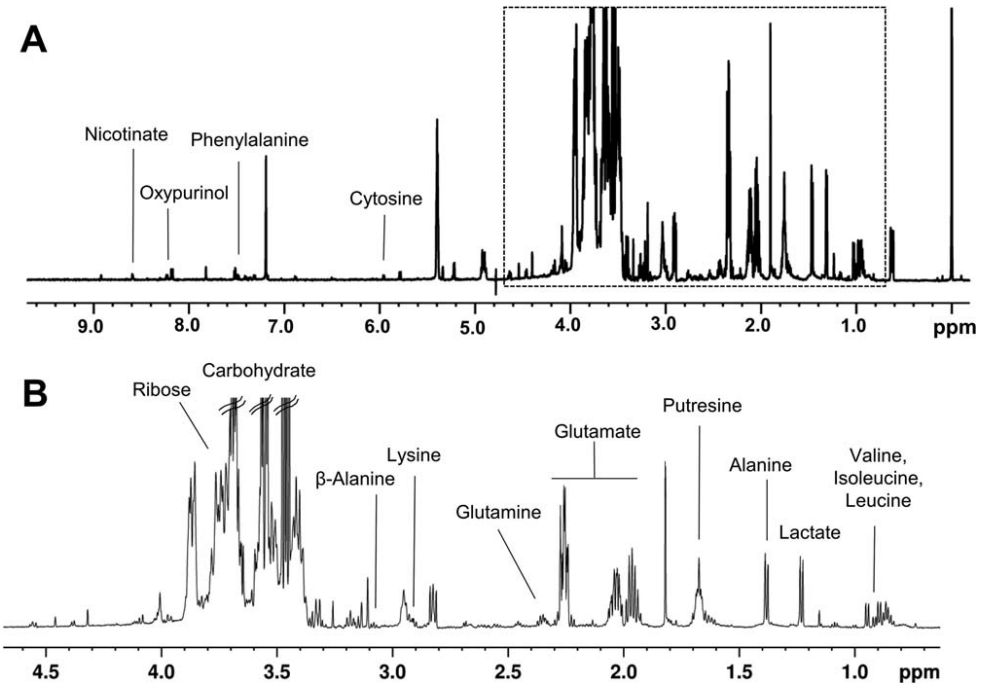

Fig. 4. Representative ^{1}H NMR spectra of intracellular metabolites obtained from As(III)-treated cells. (A) Full spectrum. (B) Close-up of region 4.7–0.7 ppm (dashed box in A). Peaks corresponding to metabolites which discriminate between control and arsenic stressed group are labeled.

integrating metabolomics information with other "omics" data.

Accumulation of three other metabolite clusters deserve discussion. If mannitol flow through glycolysis becomes stymied, a gluconeogenic-type flow to glucose-1-P can reasonably be envisioned, which then leads directly to maltose synthesis. Intermediates between mannitol and glucose-1-P were not observed, but the increased concentration of several maltose variants strengthens the view that carbon flows in this path under these circumstances. Carbohydrate synthesis could potentially be viewed as a carbon storage strategy under these conditions where possible synthesis of the more normal storage compound, poly-β-hydroxybutyrate, would be expected to be constrained due to reduced levels of its precursor, acetyl-CoA.

The proposed routing of carbon from glycolysis to phenylalanine and tryptophan via the shikimate pathway is consistent with the above discussion regarding a metabolic logjam at pyruvate. The lack of MS- or NMR-based evidence of several intermediates clearly introduces some uncertainty, however, the key end product of this pathway and immediate precursor to phenylalanine, chorismate, was observed. Significant increases in both phenylalanine and tryptophan are consistent with the proposed carbon flow.

Another consistency among metabolite changes under the experimental conditions concerns oxypurinol, hypoxanthine and xanthine (Fig. 6). Hypoxanthine is the direct precursor of xanthine, but the xanthine oxidase reaction is inhibited by arsenite (George and Bray, 1983; Hille *et al.*, 1983). Oxypurinol is another precursor of hypoxanthine (Sokol *et al.*, 1998; Boer *et al.*, 2004; Springer *et al.*, 2013) and it was found by NMR to be increased (Table 2). An increase in both xanthine oxidase inhibitors is consistent with the significant decrease in xanthine (Table 2).

As a final point, we comment on the general pattern of metabolite changes and lack of identification. Non-polar compounds dominated total MS feature counts (Figs. 1 and 2) as well as statistically significant changes (Fig. 2). Aside from at least some technical issues that may have biased metabolite extraction efficiency, this identification disconnect no doubt also links to the near absence of arsenical compounds in metabolite databases. Advances toward structural characterization of compounds containing arsenic will obviously be an important prerequisite to allow for efficient identification of such compounds. Numerous arsenolipids have been identified and characterized in micro- and macro-algae as well as higher marine organisms (Dembitsky and Levitsky, 2004), but progress with bacteria lags far behind and represents an important topic for bacteria – arsenic interaction research.

Experimental procedures

Materials and chemicals

Molecular weight cutoff (MWCO) spin filters (100 KDa and 3 KDa) were purchased from Pall Corporation (Port Washington, NY). Microcentrifuge tubes, NMR tubes and conical tubes were purchased from VWR (Radnor, PA), Bruker Daltonics (Billerica, MA) and Thermo-Fisher Sci. (Pittsburgh, PA) respectively. Disodium hydrogen phosphate, monosodium phosphate, ammonium acetate, sodium arsenite, sodium chloride, formic acid (FA), 4,4-dimethyl-4-silapentane-1-sulfonic

Table 2. Metabolites identified by NMR. Metabolites tagged by "*" were also identified by LC-MS.

Metabolite	Fold change	*p*-Value	VIP	Regulation
2′-Deoxyinosine	1.2	0.06	1.01	up
2-Hydroxy-3-methylvalerate	0.9	0.37	0.50	down
3-Methyl-2-oxovalerate	1.1	0.18	0.70	up
Acetate	1.0	0.92	0.09	up
L-Alanine	1.3	0.00	1.41	up
Choline	1.2	0.04	0.95	up
Cytosine*	2.0	0.01	1.18	up
Ethanol	1.0	0.22	0.68	
Formate	1.0	0.59	0.26	up
Fumarate	0.8	0.25	0.72	down
Gallate	1.0			
Glucose	1.0	0.79	0.03	down
L-Glutamate*	1.3	0.01	1.18	up
Glutamine	3.4	0.00	1.30	up
Glycerol	1.1	0.54	0.36	up
Hypoxanthine*	1.9	0.02	0.93	up
Imidazole	1.8	0.00	1.35	up
L-Isoleucine	1.6	0.01	1.07	up
Lactate	2.1	0.00	1.39	up
L-Leucine	1.8	0.00	1.20	up
L-Lysine*	1.7	0.00	1.34	up
Malate	0.8	0.23	0.71	down
Maltose	1.3	0.36	0.44	up
Mannitol	1.0	0.79	0.07	down
Methanol	1.6	0.47	0.21	up
Methionine	1.2	0.20	0.71	up
$NADP^+$	1.0			
Nicotinate	1.5	0.00	1.37	up
Oxypurinol	3.4	0.01	1.27	up
Phenylalanine*	1.5	0.02	1.21	up
Putrescine	1.5	0.00	1.29	up
D-Ribose	1.4	0.03	1.11	up
Tyrosine	1.3	0.04	1.04	up
Uracil	1.4	0.05	0.90	up
L-Valine*	2.0	0.00	1.41	up
B-Alanine	1.5	0.00	1.44	up

acid (DSS), deuterium oxide (D_2O) and all culture medium components were purchased from Sigma (St. Louis, MO). HPLC-grade water, acetonitrile (MeCN) and methanol (MeOH) were purchased from Burdick and Jackson (Morristown, NJ) and EMD Chemicals (Gibbstown, NJ) respectively.

Cell culturing

A single colony of *A tumefaciens* (strain 5A) (Macur *et al.*, 2004), was picked and grown aerobically for 24 h at 30°C in 50 ml of minimal mannitol ammonium medium ($MMNH_4$) (Somerville and Kahn, 1983). The cells were centrifuged for 10 min at 3500×*g*, washed 3X with 20 ml of 0.85% NaCl solution and re-suspended in fresh $MMNH_4$ containing 50 uM Pi. Aliquots of the stock culture were then used to start ten new 50 ml cultures with a starting OD_{600} of 0.1 in $MMNH_4$ 50 uM Pi medium. Five of the ten cultures were supplemented with 100 μM As(III) for arsenic stress testing, while another five cultures were kept as controls. Each culture was then grown for an additional 6 h at 30°C, centrifuged for 10 min at 3500×*g* and the cell pellet rapidly rinsed twice with 20 ml of ice cold 0.85% NaCl solution. Cell pellets were re-suspended in the same saline solution and the optical OD_{600} samples were taken such that each contained 200 ± 5 mg of final pellet biomass. Additionally, aliquots of each sample were plated $MMNH_4$ agar to allow for normalization using colony-forming units (CFU). Samples for metabolite extraction were stored at −80°C until further use.

Metabolite extraction

Intracellular metabolites for LC-MS and ^{1}H NMR analysis were extracted similar to that described by Heinemann, Hamerly, *et al.* (2014). In brief, cells were broken using two freeze/thaw cycles in liquid nitrogen followed by 5 min sonication on ice. Cells were incubated in a 50% aqueous (v/v) MeOH solution for 30 min at −20°C and cellular debris removed by centrifugation at 20 000×*g* for 15 min at −9°C. Supernatants were directly transferred to pre-washed 100 KDa MWCO filters and centrifuged at 13 000×*g* for 20 min at 4°C. The MWCO membranes were washed twice with 100 μl of the 50% MeOH solution and each time centrifuged as above. The filtrates of each sample were combined and transferred into pre-washed 3 KDa MWCO filters and the filtration procedure was repeated as described for the 100 KDa MWCO filters. The final metabolite extracts were dried under reduced pressure and stored at −80°C before spectroscopic analysis. Spin filters were washed twice with 50% MeOH solution before use for sample processing. No significant contamination from the filter membrane was observed in blank samples upon treatment with 50% MeOH solution.

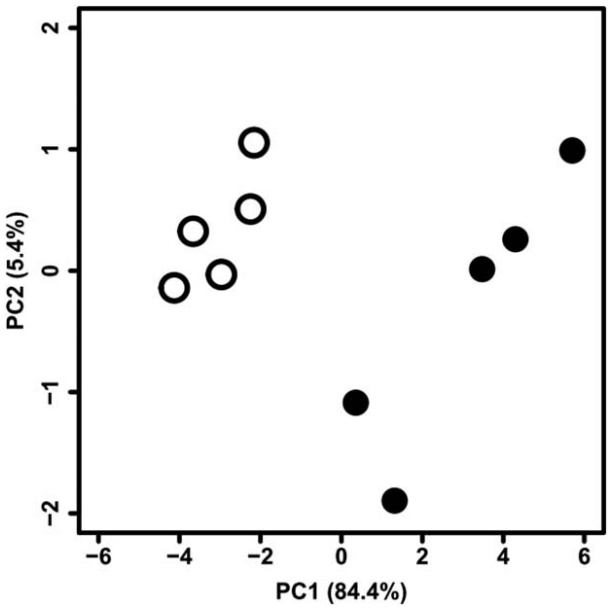

Fig. 5. PCA of ^{1}H NMR metabolomics data comparing samples collected from control (black dots) and arsenic stressed (black circles) cells. Plot is based on the metabolites listed in Table 2 with VIP score >1.

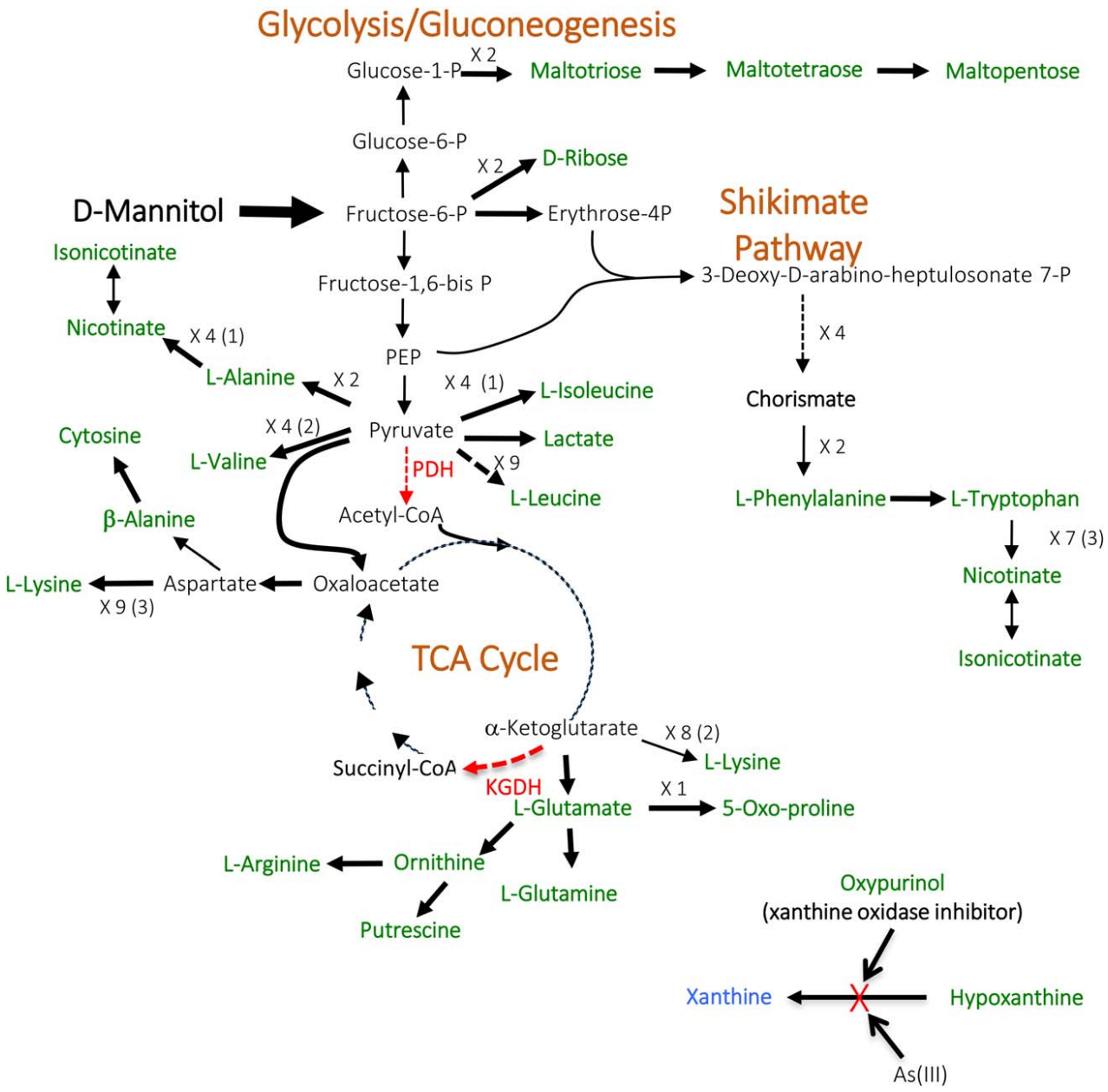

Fig. 6. Model depicting the most parsimonious explanation of influence of As(III) on carbon metabolism with mannitol being the initial substrate. Green text indicates metabolites increased in abundance, blue text indicates some of the metabolites decreased in concentration. When multiple intermediates are involved between illustrated metabolites, the number of reactions is shown; e.g. ×3, with the number of intermediates identified shown in parentheses. Red dashed vector arrows indicate reactions suggested to be inhibited by As(III) (PDH = pyruvate dehydrogenase; KGDH = α-ketoglutarate dehydrogenase). Black dashed vector arrows indicate potential pathways that involve more than two intermediates, but none of which could be identified in the MS/MS analysis. All reaction steps were derived from KEGG pathway maps.

LC-MS instrumentation and data acquisition

LC-MS based analysis was conducted on an Agilent 1290 UPLC system coupled to an Agilent 6538 Q-TOF Mass Spectrometer (Agilent Technologies, Santa Clara, CA). Two columns with orthogonal chemistry (polar and non-polar) were used to separate metabolite molecules before spectroscopic analysis. For LC-MS (non-polar) analysis, the metabolite extracts were re-suspended in 50 μl 50% aqueous (v/v) MeOH and 10 μl of sample was injected into a Zorbax RRHD Eclipse Plus (150 mm × 2.1 mm; 1.8 μm) reverse phase C18 column (Agilent Technologies, (Santa Clara, CA)). Gradient conditions for metabolite elution were as follows: 0 – 2 min, 2% B; 2 – 28 min, 2–65% B; 28 – 33 min, 65–98% B; 33 – 33.01 min, 98–2% B; 33.01–35 min, 2% B, with flow rate 0.7 ml/min and temperature of 50°C, where eluent A was 0.1% aqueous FA and eluent B was 0.1% FA in MeCN. For

LC-MS (polar) analysis, 10 μl of a 10-fold dilution of metabolite extract was injected into a Cogent Diamond Hydride HILIC column (150 mm × 2.1 mm, 4 μm, 100 Å, Microsolv Technology Corporation (Eatontown, NJ)). Gradient conditions for metabolite elution were as follows: 0 − 1 min, 99% B; 1 − 3 min, 99% B; 3 − 20 min, 99–69% B; 20 − 22 min, 69–30% B; 22–22.1 min, 30–99% B; 22–25 min, 99% B with the flow rate 0.6 ml/min and temperature of 25°C, were eluent A was 10 mM aqueous CH_3COONH_4 and eluent B was 10 mM CH_3COONH_4 in 95% MeCN. Mass spectrometry analysis was conducted in positive ion mode, with a capillary voltage of 3500 V, a fragmenting voltage of 120 V and a skimmer voltage of 45 V. Drying gas temperature was 350°C with a flow of 12 L/min and the nebulizer set to 55 psi. Spectra were collected at a rate of 1 spectrum/s over 50–1700 *m*/*z* range. For MS/MS, the scan range was 50–1300 *m*/*z* (auto MS/MS) or 50–800 *m*/*z* (targeted MS/MS) with isolation width 4 *m*/*z* and an acquisition rate 1spectrum/s. The collision energy was fixed at 35 V in targeted MS/MS mode while a linear voltage gradient was applied for molecules fragmentation in auto MS/MS experiment. Data acquisition and spectral analysis were done using MassHunter (Qualitative Analysis version B.04.00, Agilent Technologies). Samples were run in randomized order and to evaluate LC-MS system performance, the quality control (QC) sample (mixture of equal values of all experimental samples) was run in the beginning, middle and end of the queue. Variations of retention time, mass accuracy and peak area of the peaks across all QC samples were determined; the retention time shift was less than 2 s (C18) and 14 s (HILIC); the calculated mass error was below 11 ppm (C18) and 2 ppm (HILIC); the relative standard deviations of peak areas were below 7% (C18) and 17% (HILIC).

LC-MS data processing, statistical analysis and metabolite identification

LC-MS raw data files were converted to MZxml format (MassHunter Qualitative Software, Agilent Technologies (Santa Clara, CA)), and uploaded to the XCMS online server (Tautenhahn, Patti, *et al*., 2012) for spectral features extraction and alignment. The predefined parameter set UPLC-Q-TOF was used for data processing with the change made to minimum and maximum peak width set to 5 s and 20 s for C18 column derived data or 40 s for HILIC column derived data. Subsequent analysis and visualization of XCMS data was performed in R 3.0.0 language and environment for statistical computing and graphics (R Development Core Team, 2011).

The tables of retention time-aligned *m*/*z* ratios of raw molecular feature intensities (Supporting Information 1 and 2) were normalized to a sample biomass and autoscaled before Principal Component Analysis (PCA). Plots were generated based on a correlation matrix using the *prcomp* function. Only molecular features with fold changes $> \pm 1.5$ and *p*-values < 0.05 were further considered as metabolites that changed in concentration. Identification of spectral features was achieved based on three criteria: isotope distribution, retention time alignment (if standard was available) and MS/MS fragmentation pattern matching to spectra reported in the Metlin database (Smith *et al*., 2005; Tautenhahn, Cho, *et al*., 2012). Metabolic pathway mapping was performed using the KEGG (http://www.genome.jp/kegg) database (Kanehisa and Goto, 2000; Kanehisa *et al*., 2014) to investigate the metabolic pathways displaying differences between control and As(III) stressed groups and facilitate biological interpretation.

NMR data acquisition and data processing

For ^{1}H NMR, metabolite extracts were re-suspended in 600 μl of buffer (10 mM NaH_2PO_4/Na_2HPO_4 containing 0.25 mM DSS in 100% D_2O, pH 7) and transferred to 5 mm NMR tubes. NMR spectra were acquired using a 600-MHz (^{1}H Larmor frequency) AVANCE III solution NMR spectrometer from Bruker Daltonics (Billerica, MA) equipped with a SampleJet™ automatic sample loading system, a 5 mm triple resonance (^{1}H, ^{15}N, ^{13}C) liquid helium-cooled TCI probe (cryoprobeTM), and Topspin™ software (Bruker version 3.2). One-dimensional proton NMR spectra were acquired using the Bruker supplied noesypr1d pulse sequence with 256 scans, using a spectral width of 9600 Hz at 25°C. Free induction decays were collected into 32K data points, with a dwell time interval of 52 μs amounting to an acquisition time of ∼1.7 s, using a 2 s relaxation recovery delay between acquisitions, and a mixing time period of 100 msec. Spectral processing was performed using the Topspin™ software. Each spectrum was manually phased, baseline corrected and a line broadening function of 0.5 Hz applied. Metabolite analysis was performed using the Chenomx NMR software (version 8.0) (Chenomx, Edmonton, AB, Canada). For metabolite identification, the Chenomx 600 MHz, version 9 small molecule library was used, and NMR spectral patterns fitted for each sample independently. Metabolite concentrations were established using the internal calibration standard DSS (at $\delta = 0.0$ ppm). Statistical analysis was performed by exporting metabolite concentrations in micromolar units from Chenomx (in a .csv format, Supporting Information 3) into MetaboAnalyst (version 3.0, www.metaboanalyst.ca), an on-line server for metabolomics data analysis (Xia *et al*., 2009; 2012). The data were normalized using CFU, $\log_{10}$-transformed and the variance autoscaled. Statistical analyses namely *t*-test, fold-change and volcano plots were calculated. PCA and partial least-squares discriminant analysis (PLS-DA) was employed to all samples. In the case of the PLS-DA analysis, the variable importance in the projection (VIP) value for each metabolite in the model was calculated and scores of >1.1 used to identify metabolites important in discriminating between control and As(III) stressed groups. The overall quality of the model was assessed by the goodness-of-fit parameter (R^2) and the predictive ability parameter (Q^2), calculated using an internal cross-validation of the data and a leave-one-out validation method respectively.

Acknowledgements

Funding for this research was provided by the National Natural Science Foundation of China (31670108) to G.W., and by U.S. National Science Foundation grants MCB-0817170 and MCB-1413321 to T.R.M. and B.B. BB also receives support from the National Institute of General Medical Sciences of the National Institutes of Health under Award Number P20GM103474. The Mass Spectrometry Facility at received funding from funding

from the Murdock Charitable Trust and NIH 5P20RR02437 of the CoBRE program. The NMR spectra included in this manuscript were recorded at Montana State University on MSU's Bruker DRX 600 NMR spectrometer. Funding for the instrument and corresponding upgrade was provided by the NIH Shared Instrumentation Grant (SIG) program (grants # 1S10RR13878 and 1S10RR026659 respectively). B.T was supported in parts with funds provided by the by the Montana Research Initiative 51040-MUSRI2015-03.

References

Abdrashitova, S.A., Mynbaeva, B.N., Aidarkhanov, B.B., and Ilyaletdinov, A.N. (1990) Effect of arsenite on lipid peroxidation and on activity of antioxidant enzymes in arsenite-oxidizing microorganisms. *Mikrobiologiya* **59:** 234–240.

Afzal, M.I., Delaunay, S., Paris, C., Borges, F., Revol-Junelles, A.M., and Cailliez-Grimal, C. (2012) Identification of metabolic pathways involved in the biosynthesis of flavor compound 3-methylbutanal from leucine catabolism by *Carnobacterium maltaromaticum* LMA 28. *Int J Food Microbiol* **157:** 332–339.

Andres, J., Arsene-Ploetze, F., Barbe, V., Brochier-Armanet, C., Cleiss-Arnold, J., Coppee, J.Y., *et al.* (2013) Life in an arsenic-containing gold mine: genome and physiology of the autotrophic arsenite-oxidizing bacterium *Rhizobium* sp. NT-26. *Genome. Biol Evol* **5:** 934–953.

Baker-Austin, C., Dopson, M., Wexler, M., Sawers, R.G., Stemmler, A., Rosen, B.P., and Bond, P.L. (2007) Extreme arsenic resistance by the acidophilic archaeon "*Ferroplasma acidarmanus*" Fer1. *Extremophiles* **11:** 425–434.

Belfiore, C., Ordoñez, O.F., and Farías, M.E. (2013) Proteomic approach of adaptive response to arsenic stress in *Exiguobacterium* sp. S17, an extremophile strain isolated from a high-altitude Andean Lake stromatolite. *Extremophiles* **17:** 421–431.

Bergquist, E.R., Fischer, R.J., Sugden, K.D., and Martin, B.D. (2009) Inhibition by methylated organoarsenicals of the respiratory 2-oxo-acid dehydrogenases. *J Organomet Chem* **694:** 973–980.

Boer, D.R., Thapper, A., Brondino, C.D., Romão, M.J., and Moura, J.J.G. (2004) X-ray crystal structure and EPR spectra of "arsenite-inhibited" *Desulfovibriogigas* aldehyde dehydrogenase: a member of the xanthine oxidase family. *J Am Chem Soc* **126:** 8614–8615.

Brown, J.L., Kitchin, K.T., and George, M. (1997) Dimethylarsinic acid treatment alters six different rat biochemical parameters: relevance to arsenic carcinogenesis. *Teratog. Carcinog. Mutagen* **17:** 71–84.

Bryan, C.G., Marchal, M., Battaglia-Brunet, F., Kugler, V., Lemaitre-Guillier, C., Lievremont, D., *et al.* (2009) Carbon and arsenic metabolism in *Thiomonas* strains: differences revealed diverse adaptation processes. *BMC Microbiol* **9:** 127.

Carapito, C., Muller, D., Turlin, E., Koechler, S., Danchin, A., Van Dorsselaer, A., *et al.* (2006) Identification of genes and proteins involved in the pleiotropic response to arsenic stress in *Caenibacter arsenoxydans*, a metalloresistant beta-proteobacterium with an unsequenced genome. *Biochimie* **88:** 595–606.

Chen, F., Cao, Y., Wei, S., Li, Y., Li, X., Wang, Q., and Wang, G. (2015) Regulation of arsenite oxidation by the phosphate two-component system PhoBR in *Halomonas* sp. HAL1. *Front Microbiol* **6:** 1–9.

Chen, W., Taylor, N.L., Chi, Y., Millar, A.H., Lambers, H., and Finnegan, P.M. (2014) The metabolic acclimation of *Arabidopsis thaliana* to arsenate is sensitized by the loss of mitochondrial lipoamide dehydrogenase2, a key enzyme in oxidative metabolism. *Plant Cell Environ* **37:** 684–695.

Cleiss-Arnold, J., Koechler, S., Proux, C., Fardeau, M.L., Dillies, M.A., Coppee, J.Y., *et al.* (2010) Temporal transcriptomic response during arsenic stress in *Herminiimonas arsenicoxydans*. *BMC Genomics* **11:** 709.

Dembitsky, V.M., and Levitsky, D.O. (2004) Arsenolipids. *Prog Lipid Res* **43:** 403–448.

Emmett, M. (2014) Acetaminophen toxicity and 5-oxoproline (pyroglutamic acid): a tale of two cycles, one an ATP-depleting futile cycle and the other a useful cycle. *Clin J Am Soc Nephrol* **9:** 191–200.

Flamigni, F., Marmiroli, S., Caldarera, C.M., Guarnieri, C.A.R.L., and Biochirnica, D. (1989) Effect of sodium arsenite on the induction and turnover of ornithine decarboxylase activity in *Erythroleukemia* cells. *Cell Biochem Funct* **7:** 213–217.

Ge, Y., Ning, Z., Wang, Y., Zheng, Y., Zhang, C., and Figeys, D. (2016) Quantitative proteomic analysis of *Dunaliella salina* upon acute arsenate exposure. *Chemosphere* **145:** 112–118.

George, G.N., and Bray, R.C. (1983) Reaction of arsenite ions with the molybdenum center of milk xanthine oxidase. *Biochemistry* **22:** 1013–1021.

González-Segura, L., Mújica-Jiménez, C., and Muñoz-Clares, R.A. (2009) Reaction of the catalytic cysteine of betaine aldehyde dehydrogenase from *Pseudomonas aeruginosa* with arsenite-BAL and phenylarsine oxide. *Chem Biol Interact* **178:** 64–69.

Haimeur, A., Guimond, C., Pilote, S., Mukhopadhyay, R., Rosen, B.P., Poulin, R., and Ouellette, M. (1999) Elevated levels of polyamines and trypanothione resulting from overexpression of the ornithine decarboxylase gene in arsenite-resistant *Leishmania*. *Mol Microbiol* **34:** 726–735.

Hall, L.L., George, S.E., Kohan, M.J., Styblo, M., and Thomas, D.J. (1997) *In vitro* methylation of inorganic arsenic in mouse intestinal cecum. *Toxicol Appl Pharmacol* **147:** 101–109.

Halter, D., Andres, J., Plewniak, F., Poulain, J., Da Silva, C., Arsène-Ploetze, F., and Bertin, P.N. (2015) Arsenic hyper tolerance in the protist *Euglena mutabilis* is mediated by specific transporters and functional integrity maintenance mechanisms. *Environ Microbiol* **17:** 1941–1949.

Heinemann, J., Hamerly, T., Maaty, W.S., Movahed, N., Steffens, J.D., Reeves, B.D., *et al.* (2014) Expanding the paradigm of thiol redox in the thermophilic root of life. *Biochim Biophys Acta* **1840:** 80–85.

Heinemann, J., Mazurie, A., Tokmina-Lukaszewska, M., Beilman, G.J., and Bothner, B. (2014) Application of support vector machines to metabolomics experiments with limited replicates. *Metabolomics* **10:** 1121–1128.

Hille, R., Stewart, R.C., Fee, J.A., and Massey, V. (1983) The interaction of arsenite with xanthine oxidase. *J Biol Chem* **258:** 4849–4856.

Jain, R., Adhikary, H., Jha, S., Jha, A., and Kumar, G.N. (2012) Remodulation of central carbon metabolic pathway in response to arsenite exposure in *Rhodococcus* sp. strain NAU-1. *Microb Biotechnol* **5:** 764–772.

Ji, G., and Silver, S. (1992) Reduction of arsenate to arsenite by the ArsC protein of the arsenic resistance operon of *Staphylococcus aureus* plasmid p1258. *Proc Natl Acad Sci USA* **89:** 9474–9478.

Jomova, K., Jenisova, Z., Feszterova, M., Baros, S., Liska, J., Hudecova, D., *et al*. (2011) Arsenic: toxicity, oxidative stress and human disease. *J Appl Toxicol* **31:** 95–107.

Kanehisa, M., and Goto, S. (2000) Kyoto encyclopedia of genes and genomes. *Nucleic Acids Res* **28:** 27–30.

Kanehisa, M., Goto, S., Sato, Y., Kawashima, M., Furumichi, M., and Tanabe, M. (2014) Data, information, knowledge and principle: back to metabolism in KEGG. *Nucleic Acids Res* **42:** D199–D205.

Kang, Y.S., Bothner, B., Rensing, C., and McDermott, T.R. (2012) Involvement of RpoN in regulating bacterial arsenite oxidation. *Appl Environ Microbiol* **78:** 5638–5645.

Kang, Y.S., Brame, K., Jetter, J., Bothner, B.B., Wang, G., Thiyagarajan, S., and McDermott, T.R. (2016) Regulatory activities of four ArsR proteins in *Agrobacterium tumefaciens* 5A. *Appl Environ Microbiol* AEM.00262–16.

Kang, Y.S., Heinemann, J., Bothner, B., Rensing, C., and McDermott, T.R. (2012) Integrated co-regulation of bacterial arsenic and phosphorus metabolisms. *Environ Microbiol* **14:** 3097–3109.

Kashyap, D.R., Botero, L.M., Franck, W.L., Hassett, D.J., and McDermott, T.R. (2006) Complex regulation of arsenite oxidation in *Agrobacterium tumefaciens*. *J Bacteriol* **188:** 1081–1088.

Koechler, S., Cleiss-Arnold, J., Proux, C., Sismeiro, O., Dillies, M.A., Goulhen-Chollet, F., *et al*. (2010) Multiple controls affect arsenite oxidase gene expression in *Herminiimonas arsenicoxydans*. *BMC Microbiol* **10:** 53.

Li, B., Lin, J., Mi, S., and Lin, J. (2010) Arsenic resistance operon structure in *Leptospirillum ferriphilum* and proteomic response to arsenic stress. *Bioresour Technol* **101:** 9811–9814.

Liu, G., Liu, M., Kim, E.H., Maaty, W.S., Bothner, B., Lei, B., *et al*. (2012) A periplasmic arsenite-binding protein involved in regulating arsenite oxidation. *Environ Microbiol* **14:** 1624–1634.

Lu, K., Abo, R.P., Schlieper, K.A., Graffam, M.E., Levine, S., Wishnok, J.S., *et al*. (2014) Arsenic exposure perturbs the gut microbiome and its metabolic profile in mice: an integrated metagenomics and metabolomics analysis. *Environ Health Perspect* **122:** 284–291.

Macur, R.E., Jackson, C.R., Botero, L.M., McDermott, T.R., and Inskeep, W.P. (2004) Bacterial populations associated with the oxidation and reduction of arsenic in an unsaturated soil. *Environ Sci Technol* **38:** 104–111.

Mukhopadhyay, R., Rosen, B.P., Phung, L.T., and Silver, S. (2002) Microbial arsenic: from geocycles to genes and enzymes. *FEMS Microbiol Rev* **26:** 311–325.

Muller, D., Lièvremont, D., Simeonova, D.D., Hubert, J.C., and Lett, M.C. (2003) Arsenite oxidase *aox* genes from a metal-resistant β-proteobacterium. *J Bacteriol* **185:** 135–141.

Muller, D., Médigue, C., Koechler, S., Barbe, V., Barakat, M., Talla, E., *et al*. (2007) A tale of two oxidation states: bacterial colonization of arsenic-rich environments. *PLoS Genet* **3:** 0518–0530.

Murphy, J.N., and Saltikov, C.W. (2007) The *cymA* gene, encoding a tetraheme c-type cytochrome, is required for arsenate respiration in *Shewanella* species. *J Bacteriol* **189:** 2283–2290.

Murphy, J.N., and Saltikov, C.W. (2009) The ArsR repressor mediates arsenite-dependent regulation of arsenate respiration and detoxification operons of *Shewanella* sp. strain ANA-3. *J Bacteriol* **191:** 6722–6731.

Ochi, T. (1997) Arsenic compound-induced increases in glutathione levels in cultured Chinese hamster V79 cells and mechanisms associated with changes in gamma-glutamylcysteine synthetase activity, cystine uptake and utilization of cysteine. *Arch Toxicol* **71:** 730–740.

Oremland, R.S., and Stolz, J.F. (2003) The ecology of arsenic. *Science (80-.)* **300:** 939–944.

Osborne, F.H., and Ehrlich, H.L. (1976) Oxidation of arsenite by a soil isolate of *Alcaligenes*. *J Appl Bacteriol* **42:** 295–305.

Pandey, S., Rai, R., and Rai, L.C. (2012) Proteomics combines morphological, physiological and biochemical attributes to unravel the survival strategy of *Anabaena* sp. PCC7120 under arsenic stress. *J Proteomics* **75:** 921–937.

Parvatiyar, K., Alsabbagh, E.M., Ochsner, U.A., Stegemeyer, M.A., Smulian, A.G., Hwang, S.H., *et al*. (2005) Global analysis of cellular factors and responses involved in *Pseudomonas aeruginosa* resistance to arsenite. *J Bacteriol* **187:** 4853–4864.

Phillips, S.E., and Taylor, M.L. (1976) Oxidation of arsenite to arsenate by *Alcaligenes faecalis*. *Appl Environ Microbiol* **32:** 392–399.

R Development Core Team (2011) R: a language and environment for statistical computing. *R Found Stat Comput* **1:** 409.

Reyes, C., Murphy, J.N., and Saltikov, C.W. (2010) Mutational and gene expression analysis of *mtrDEF*, *omcA* and *mtrCAB* during arsenate and iron reduction in *Shewanella* sp. ANA-3. *Environ Microbiol* **12:** 1878–1888.

Rosen, B.P. (2002) Transport and detoxification systems for transition metals, heavy metals and metalloids in eukaryotic and prokaryotic microbes. *Comparative Biochemistry and Physiology Part A: Molecular & Integrative Physiology*. **133:** pp. 689–693.

Sacheti, P., Patil, R., Dube, A., Bhonsle, H., Thombre, D., Marathe, S., *et al*. (2014) Proteomics of arsenic stress in the gram-positive organism *Exiguobacterium* sp. PS NCIM 5463. *Appl Microbiol Biotechnol* **98:** 6761–6773.

Saltikov, C.W., and Newman, D.K. (2003) Genetic identification of a respiratory arsenate reductase. *Proc Natl Acad Sci USA* **100:** 10983–10988.

Sanchez-Riego, A.M., Lopez-Maury, L., and Florencio, F.J. (2014) Genomic responses to arsenic in the cyanobacterium *Synechocystis* sp. PCC 6803. *PLoS One* **9:** e96826.

Santini, J.M., Sly, L.I., Schnagl, R.D., and Macy, J.M. (2000) A new chemolithoautotrophic arsenite-oxidizing bacterium isolated from a gold mine: phylogenetic, physiological, and preliminary biochemical studies. *Appl Environ Microbiol* **66:** 92–97.

Shi, H., Shi, X., and Liu, K.J. (2004) Oxidative mechanism of arsenic toxicity and carcinogenesis. *Mol Cell Biochem* **255:** 67–78.

Silver, S., and Phung, L.T. (2005) Genes and enzymes involved in bacterial oxidation and reduction of inorganic arsenic. *Appl Environ Microbiol* **71:** 599–608.

Smith, C.A., O'maille, G., Want, E.J., Qin, C., Trauger, S.A., Brandon, T.R., *et al*. (2005) METLIN: a metabolite mass spectral database. *Ther Drug Monit* **27:** 747–751.

Sokol, R.J., Devereaux, M.W., and Khandwala, R. (1998) Effect of oxypurinol, a xanthine oxidase inhibitor, on hepatic injury in the bile duct-ligated rat. *Pediatr Res* **44:** 397–401.

Somerville, J.E., and Kahn, M.L. (1983) Cloning of the glutamine synthetase I gene from *Rhizobium meliloti*. *J Bacteriol* **156:** 168–176.

Springer, J., Tschirner, A., Hartman, K., Von Haehling, S., Anker, S.D., and Doehner, W. (2013) The xanthine oxidase inhibitor oxypurinol reduces cancer cachexia-induced cardiomyopathy. *Int J Cardiol* **168:** 3527–3531.

Stolz, J.F., and Oremland, R.S. (1999) Bacterial respiration of arsenic and selenium. *FEMS Microbiol Rev* **23:** 615–627.

Tautenhahn, R., Cho, K., Uritboonthai, W., Zhu, Z., Patti, G.J., and Siuzdak, G. (2012) An accelerated workflow for untargeted metabolomics using the METLIN database. *Nat Biotechnol* **30:** 826–828.

Tautenhahn, R., Patti, G.J., Rinehart, D., and Siuzdak, G. (2012) XCMS online: a web-based platform to process untargeted metabolomic data. *Anal Chem* **84:** 5035–5039.

Thomas, J. A., Chovanec, P., Stolz, J.F., and Basu, P. (2014) Mapping the protein profile involved in the biotransformation of organoarsenicals using an arsenic metabolizing bacterium. *Metallomics* **6:** 1958–1969.

Tokmina-Lukaszewska, M., Movahed, N., Lusczek, E.R., Mulier, K.E., Beilman, G.J., and Bothner, B. (2014) Transformation of UPLC-MS data overcomes extreme variability in urine concentration and metabolite fold change. *Curr Metabolomics* **2:** 78–87.

Wang, Q., Qin, D., Zhang, S., Wang, L., Li, J., Rensing, C., *et al*. (2015) Fate of arsenate following arsenite oxidation in *Agrobacterium tumefaciens* GW4. *Environ Microbiol* **17:** 1926–1940.

Weiss, S., Carapito, C., Cleiss, J., Koechler, S., Turlin, E., Coppee, J.Y., *et al*. (2009) Enhanced structural and functional genome elucidation of the arsenite-oxidizing strain *Herminiimonas arsenicoxydans* by proteomics data. *Biochimie* **91:** 192–203.

Xia, J., Mandal, R., Sinelnikov, I.V., Broadhurst, D., and Wishart, D.S. (2012) MetaboAnalyst 2.0-a comprehensive server for metabolomic data analysis. *Nucleic Acids Res* **40:** 127–133.

Xia, J., Psychogios, N., Young, N., and Wishart, D.S. (2009) MetaboAnalyst: a web server for metabolomic data analysis and interpretation. *Nucleic Acids Res* **37:** 652–660.

Supporting information

Additional Supporting Information may be found in the online version of this article at the publisher's web-site:

Supporting Information 1. The table of retention time-aligned m/z ratios of raw molecular feature intensities saved in .xlsx format as C18 XCMS data output.

Supporting Information 2. The table of retention time-aligned m/z ratios of raw molecular feature intensities saved in .xlsx format as HILIC XCMS data output.

Supporting Information 3. The table of identified metabolites and their concentrations exported in .csv format from Chenomx.